Quantifying human upper limb stiffness responses based on a computationally efficient neuromusculoskeletal arm model

Maria Sapounaki[1,2], Pierre Schumacher[2,4], Winfried Ilg[2], Martin Giese[2], Christophe Maufroy[4,5]
Andreas Bulling[6], Syn Schmitt[7], Daniel F.B. Haeufle[1,2,*], and Isabell Wochner[1,*]

Abstract— Activities of daily living such as drinking and eating can be severely impaired for patients suffering from neurodegenerative diseases. One promising solution are assistive devices that apply corrective forces while still allowing the intended movements. However, real-time estimation of the required forces requires a detailed understanding of the limb's impedance characteristics. Here, we test and validate the stiffness response of a computationally efficient neuromusculoskeletal arm model and its response to various force perturbations. We demonstrate that the arm model predicts stiffness characteristics that closely match experimental data recorded from humans and presents real-time applicability, allowing for implementation in practical scenarios and. Additionally, we predict the stiffness response for novel force levels and arm configurations. In the future, these predictions could be used to estimate corrective forces for assistive devices in real-time.

I. Introduction

Neurodegenerative diseases may profoundly impact daily activities such as eating, drinking, and handling objects due to motor control impairments like tremors or overshooting movements. Assistive devices emerge as a promising solution, capable of mitigating these effects by providing real-time corrective forces. Predicting impedance of the human upper limb in real-time is crucial to determine adequate assistive fores. Impedance describes the resistance of the arm to external forces and can be measured by applying perturbations to the hand [1]. The resulting displacement or hand force allows us to estimate physical parameters such as arm stiffness, viscosity, and inertia [2]. Stiffness ellipses (SE)—primarily characterized by their size (i.e. the area of the ellipse), shape (i.e. the ratio between the length of the major & minor axis of the ellipse), and orientation (i.e. the direction of the major axis about a fixed coordination system)—serve as visual representations of impedance [3]–[5]. While experimentally measuring arm stiffness is essential to validate upper limb models, experimental assessments of arm stiffness often have limitations, due to a limited number of participants, measured force levels, or measured limb postures.

Therefore, model-based studies employing musculoskeletal models to simulate the human arm's response to externally applied forces present a promising alternative. While such approaches offer a comprehensive characterization of upper limb impedance properties, most studies have relied on simplified models, limiting the inclusion of crucial details such as the number of used muscles or muscle stiffness properties [6], [7]. Recently, a more complex computational neuromusculoskeletal model integrated into OpenSim has been employed for a more detailed assessment of the mechanical impedance [8]. Despite this model's ability to closely mimic human arm behavior observed in experimental settings, its computational efficiency may not be suitable for the integration of real-time control in assistive devices.

Thus, the purpose of this study is to test, for the first time, whether the computationally efficient arm model in MuJoCo physics engine [9], [10] can accurately predict stiffness ellipses as presented in experimental in-vivo studies. We test the prediction for different force levels and different arm configurations targeted at activities of daily living. Our study provides novel data to estimate corrective forces for assistive devices and may be a starting point to predict them in real-time.

II. Related Work

Various studies have conducted experiments or numerical simulations to estimate the impedance characteristics of the upper limb [3], [4], [8], [11]–[13]. However, to the best of our knowledge, most of these studies did not present stiffness values directly but rather present their results as graphical representations, i.e. stiffness ellipses which make precise comparisons difficult. Thus, we tried to digitize and extract presented values and summarized them as a comprehensive comparison in Table I, which encapsulates the core details of each experiment in terms of duration, level and direction of the applied force and the stiffness values.

Concerning the direction of the external perturbation, in the majority of the cases, an approach involving eight different angles (deviating by 45°) per experiment was chosen. An exception is the study by [13] where

[1]Institute of Computer Engineering (ZITI), Heidelberg University, Germany. [2]Hertie Institute for Clinical Brain Research, and Werner Reichard Centre for Integrative Neuroscience, University of Tübingen, Tübingen, Germany. [3]Max-Planck Institute for Intelligent Systems, Tübingen, Germany. [4]Institut for Industrial Manufacturing and Management (IFF), University of Stuttgart, Germany. [5]Fraunhofer Institute for Manufacturing Engineering and Automation (IPA), Germany. [6]Institute for Visualization and Interactive Systems, University of Stuttgart, Germany. [7]Institute for Modelling and Simulation of Biomechanical Systems, University of Stuttgart, Germany. *corresponding authors with equal contributions: isabell.wochner@ziti.uni-heidelberg.de and daniel.haeufle@ziti.uni-heidelberg.de

This work was financed by the Baden-Württemberg Stiftung in the scope of the AUTONOMOUS ROBOTICS project iAssistADL granted to WI, MG, SynS, and DH

the perturbation followed only three force directions (from elbow-to-hand line, from hand-to-shoulder line, and force halfway of the latter two). The duration of the external force application ranges between 10 ms and 2 s, while the magnitude and the type of the applied force vary from 2 N to 20 N and from stochastic to predefined perturbations, correspondingly. The resulting displacement of the endpoint is in the order of 2 mm-108 mm. Finally, the recorded stiffness is mainly between 400 N/m and 700 N/m for holding a posture. During movements, stiffness of up 5000 N/m have been reported [14].

III. Methods

A. Musculoskeletal model

In this paper, we used the arm model described by Ikkala et al. [10], who adapted it from [18]. It is a rigid-body arm model that contains 26 Hill-type muscle actuators with non-elastic tendons, 17 segments, and has five degrees of freedom (DOFs) with physiological joint axis orientations, and joint angle limits. Both research works [10], [18] that used the "MOBL ARMS" model claimed that the model behavior closely resembles the reaction to external forces of a biological arm.

B. Simulation Setup

We conducted simulation experiments via Python and MuJoCo to control the simulation environment and arm model. We performed the analysis of the data extracted from the simulation in Matlab.

The experiments included four different arm configurations (see Fig. 1 and Table II). They were chosen to represent a variety of arm configurations; a relaxed position ((a) represented by the Initial position), a position representing reaching for objects ((b) Extended position), a position representing eating ((c) Eating Position) and one position representing the main configuration tested in previous experiments ((d) Literature position). Each of these equilibrium configurations was reached by setting a vector of constant muscle stimulation values applied as open-loop signals. Note that these stimulation values were found heuristically to resemble the desired each arm configuration. A given vector of constant muscle stimulations results in a unique equilibrium position (in the absence of external loads). In each of these positions, we applied perturbation forces in 8 different directions in 45° steps and with different force levels ranging between 0.5 N-25 N. The constant forces were applied for 100 ms.

Angle \ Arm Conf.	Initial	Extended	Eating	Literature
Shoulder angle	4°	69°	82°	75°
Elbow angle	87°	22°	129°	93°

TABLE II: Joint (shoulder and elbow) angles for each arm configuration.

In our analysis, we wanted to focus on the stiffness prediction by the muscles and exclude possible contributions of the joint limit torques. To ensure this, we excluded perturbation force levels for an arm configuration where joint limit sensors detected constraint force >8 Nm in one or more perturbation directions.

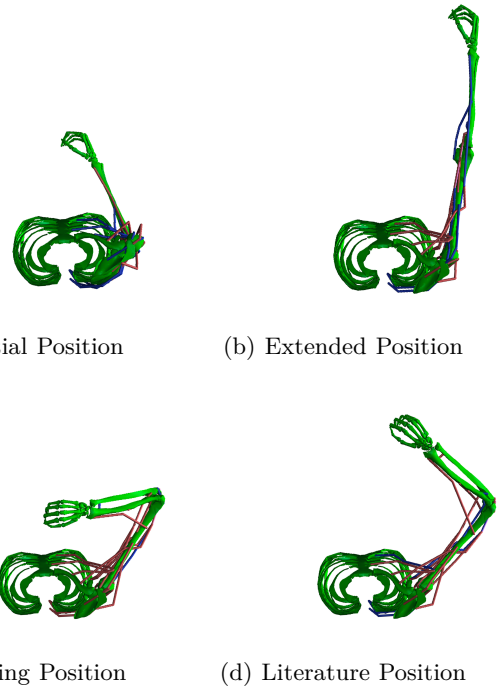

(a) Initial Position (b) Extended Position

(c) Eating Position (d) Literature Position

Fig. 1: Figures 1a-1d depict the postures achieved by the different levels of muscle activation.

C. Computation of Stiffness

Previous studies [11], [15] demonstrated that when the arm is stabilized at an equilibrium posture, the endpoint response to a perturbation could be described by an impedance model factoring in inertia, $\mathbf{M}_{end}$, viscosity, $\mathbf{B}_{end}$, and endpoint stiffness, $\mathbf{K}_{end}$ as shown in Eq. 1. $\mathbf{F}_{end}$ represents the force vector caused by the enforced perturbation displacement $d\mathbf{x}$.

$$\mathbf{M_{end}}\mathbf{d\ddot{x}} + \mathbf{B_{end}}\mathbf{d\dot{x}} + \mathbf{K_{end}}\mathbf{dx} = -\mathbf{dF_{end}} \quad (1)$$

where $\mathbf{dx} = \mathbf{x(t)} - \mathbf{x_0}$ and $\mathbf{dF} = \mathbf{F(t)} - \mathbf{F_0}$. $\mathbf{x_0}$ and $\mathbf{F_0}$ denote the position coordinates and the force prior to the onset of the perturbation, correspondingly. For small and short perturbations, $\mathbf{K_{end}}$, $\mathbf{M_{end}}$, and $\mathbf{B_{end}}$ were assumed to be constant and exhibit posture-dependent variations [11], [16]. Consequently, despite the inherent nonlinearity of the neuromuscular system, linear estimation may be suitable for such perturbations [17]. Based on [12], Eq. 1 can be simplified as follows:

$$\mathbf{K_{end}}\mathbf{dx} = -\mathbf{dF_{end}} \quad (2)$$

After measuring the displacements $\mathbf{dx}$ caused by a known unit of force $\mathbf{F}$, we calculated the endpoint

TABLE I: Comprehensive comparison of existing studies presenting impedance characteristics of the human arm.

Work	Direction	Duration	Force Level [N]	Displacement [mm]	Stiffness [N/m]
[11]	8 different randomly chosen angles	400 ms	4	10 (simulations) 5 (human exp)	$K_{xx} = [81.2, 257.9]$ $K_{yx} = [-291.5, -82.6]$ $K_{xy} = [-277.9, -86.7]$ $K_{yy} = [107.5, 448.2]$
[12]	8 different (45°)	100 ms	[5, 10, 15, 20]	7	$K_{xx} = [90, 95]$ $K_{yx} = [65.5, 72.8]$ $K_{xy} = [-78.1, 86.6]$ $K_{yy} = [151.9, 189.1]$
[4]	8 different (45°)	300 ms	2	7	Major axis: [450, 750] Minor axis: [200, 350]
[8]	8 different (45°)	1.2 s	2	2	Major axis: [400, 700] Minor axis: [20, 350]
[13]	3 directions: (1) force directed from elbow-to-hand line (2) force directed form hand-to-shoulder line (3) force halfway of (1) & (2)	-	a bandlimited stochastic position perturbation $F_x = [-10, 10]$ $F_y = [-30, -10]$ x, y nearly independent	10	Major axis: [1700, 2100] Minor axis: [50, 350]
[14]	3 directions: 45° 165° 285°	50 ms	[3, 4, 5]	-	Major axis: [1000, 5000] Minor axis: [50, 400]
[1]	0.05° to 2.3° for the shoulder 0.025° to 3.9° for the elbow	120 ms	-	either 4 or 8	-
[15]	8 different (45°)	1.5 - 2 s	F_x=[-3,1.5] F_y=[-2,4]	d_x=[-6,-4] d_y=[4,7]	Major axis: [600, 1000] Minor axis: [100, 400]
[16]	8 different (45°)	0.3 s	-	6-8	Major axis: [200, 600] Minor axis: [30, 170]
[17]	randomly chosen from the set $F_y = k(2\pi/8), k = 1..8$	300 ms	position perturbations $F_x = [-3, 2] F_y = [-2, 4]$	8	-

stiffness matrix, $\mathbf{K_{end}}$, based on Eq. 2, considering the data from all perturbations in all directions for a given arm configuration and force level (least square optimization). Once $\mathbf{K_{end}}$ was computed, it was then multiplied by a unit displacement matrix that contained the sin and cos functions, as seen in Eq. 3, to calculate the stiffness ellipse.

$$\begin{bmatrix} \mathbf{F_x^K}(t) \\ \mathbf{F_y^K}(t) \end{bmatrix} = \mathbf{K_{end}} \cdot \begin{bmatrix} \cos(t) \\ \sin(t) \end{bmatrix}, \text{where} \quad 0 < t < 2\pi \tag{3}$$

Acknowledging the importance of the stiffness ellipses' characteristics in relation to the existing literature, the orientation of the major axis, ϕ, shape, s, and area, A, of each ellipse were computed [13]. Orientation corresponds to the angle (measured in rad) that is formed by the major axis of each stiffness ellipse regarding the shoulder joint, shape is a dimensionless metric defined as the ratio of the minor axis length to the major axis length and area is the space that is occupied by each ellipse. For the sake of simplicity, the orientation of the major axis, ϕ, will be called orientation.

$$\phi = \arctan\left(\frac{U_{max\_y}}{U_{max\_x}}\right) \tag{4}$$

$$s = \frac{a_{min}}{a_{max}}, \tag{5}$$

$$A = \pi a_{min} a_{max} \tag{6}$$

U_{max_x} and U_{max_y} are the elements of matrix $\mathbf{U}$, obtained by Singular Value Decomposition of the $\mathbf{K_{end}}$ matrix [19]. The half axis lengths are $a_{min} = \sqrt{\lambda_{min}(\mathbf{K_{end}^T})}$ and $a_{max} = \sqrt{\lambda_{max}(\mathbf{K_{end}^T})}$, where $\lambda(\cdot)$ denotes the eigenvalue operator.

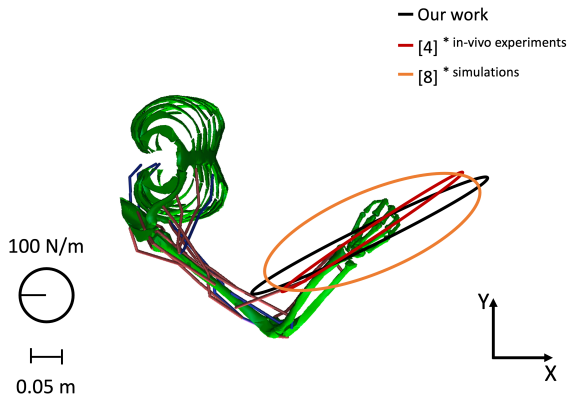

Fig. 2: Graphical representation of the stiffness ellipses, when applied force equals 2 N, obtained from the simulation of this work in comparison with the corresponding ellipses extracted from the literature (red and orange ellipse were digitized from [4] and [8]).

IV. Results

In the following, we show the results of perturbing the arm model for different arm configurations with varying force perturbation levels and present the resulting stiffness values. A graphical representation of the stiffness ellipses from our arm model in comparison to literature values extracted from [4] and [8] demonstrate the adequacy of our approach to predict upper limb stiffness values (see Fig. 2). We chose force perturbation of 2 N as the reference value for this comparison, as this force level is most commonly chosen in experimental studies (see also Table I). Both the size and orientation of the predicted stiffness ellipses closely match previously presented values from the literature.

In previous studies, most experimental work only recorded upper limb impedance values for one specific

force level. To understand the influence of the perturbation force, we applied different constant force levels to the Literature arm configuration and investigated the final hand position (x- and y-coordinates) that the model reached after an external perturbation was applied for 100 ms for forces between $0.5-3$ N (see Fig. 3a). Note that, we also tested higher forces and they led to even higher and more distorted displacements, here not shown for clarity. The final hand displacement changes depending on the applied external forces: The larger the applied perturbation force, the larger the resulting hand displacement. The orientation of the corresponding stiffness ellipses is orthogonal to the position data, and the larger the applied force, the smaller the resulting shape of the ellipse (Fig. 3b). Stiffness values for the Literature arm position fluctuate from -53 N/m to 777 N/m across the range of the investigated force magnitude (Table III). Note that, lower external perturbations result in higher stiffness values, and their non-diagonal elements of the $\mathbf{K_{end}}$ tend to approach equality, resulting in an increased level of symmetry. Forces higher than 5 N/m formulate negative non-diagonal elements with remarkably lower stiffness values.

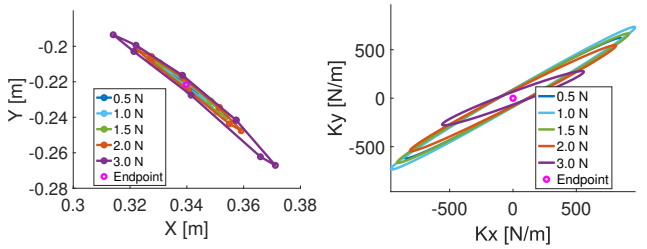

(a) Hand position data (b) Stiffness ellipses

Fig. 3: Raw position data and stiffness ellipses for the Literature arm configuration across different external forces.

We also varied the equilibrium position of the arm to which the perturbation was applied. In all four investigated arm configurations (Initial, Extended, Eating and Literature position), we observe that smaller levels of applied forces result in smaller displacements (Fig. 4). Notably, for smaller force values (up to 1.5 N), the eight tested perturbation directions and the resulting displacements form an ellipse, which was consistent with in-vivo experiments. The applied forces increase beyond a threshold, the model deviates from the anticipated behavior observed at lower force levels and the linear approximation hypothesis underlying Eq. 1 does not hold anymore (see R^2 values in Table III).

The results demonstrate a clear influence of the arm configuration and the applied force level on the orientation and magnitude of the stiffness (see Fig. 5a and 4d). All four arm configurations seem to follow a general pattern: as the external force increases, the area of the SEs declines while their shape mostly remains at the same level and the angle denoting their orientation appears to

TABLE III: Stiffness matrix values ([N/m]) for the Literature configuration per applied force level and the corresponding R^2.

Force [N]	$\boldsymbol{K_{xx}}$	$\boldsymbol{K_{xy}}$	$\boldsymbol{K_{yx}}$	$\boldsymbol{K_{yy}}$	$\boldsymbol{R^2}$
0.5	690.7	446.9	501.8	433.2	0.90
0.75	756.8	516.8	555.9	489.9	0.97
1	777.0	536.5	570.7	503.8	0.98
1.25	766.9	520.1	560.1	487.8	0.96
1.5	741.1	487.1	536.3	457.7	0.92
1.75	706.6	444.6	505.3	419.8	0.87
2	664.4	396.4	468.2	377.3	0.82
2.5	564.4	289.6	383.0	285.8	0.75
3	469.6	192.6	302.9	203.1	0.68
5	153.7	-35.9	34.7	11.3	0.45
7.5	135.7	-23.0	22.7	25.0	0.45
10	134.9	-20.3	17.1	28.2	0.59
12.5	99.5	-6.9	-6.9	31.4	0.52
15	53.4	-30.2	-45.5	15.6	0.54
17.5	65.6	-13.7	-52.8	22.6	0.54
20	109.0	51.1	-47.2	50.0	0.45
25	236.5	198.0	-24.0	107.3	0.41

vary in a way that is dependent on the in-question arm configuration. This holds true up to a certain force limit which is correlated to the arm configuration. Beyond this threshold, a notable divergence in kinematic behavior emerges, and additionally, R^2 dropped below 0.8 (Table III) highlighting the inadequacy of the ellipsoidal model for stiffness calculation under these conditions. However, for the Extended arm position (Fig. 4b), at least one of the joint limits is exceeded for each angle of all the tested force levels in this arm configuration, which influences their ellipsoidal representation (Fig. 5b).

Comparing the different arm configurations (Fig. 6), when an external force of 2 N was applied, show that the Literature arm position (red line) and the Initial arm position (blue line) exhibit significantly smaller areas compared to the stiffness ellipse corresponding to the Eating position (purple line), which displayed a larger size and higher eccentricity. Note that, we chose this reference perturbation level of 2 N, as this force level was most commonly chosen in experimental studies (see also Table I).

Additionally, we investigated the computationally efficiency of the model. As reported in [20], the arm model used in MuJoCo runs roughly 600 times faster than the original OpenSim model [18]. To further test its real-time applicability, we evaluated the averaged run time over 1000 forward simulations: On average, a reaching movement with a 1 s simulation duration takes 0.0162 s on a standard laptop equipped with an AMD Ryzen 7 PRO 4750U processor and 16 GB RAM.

V. Discussion

In this study, we conducted a detailed investigation of the upper limb stiffness responses to a range of external perturbations in four arm configurations using a computationally efficient arm model in MuJoCo.

We showed that our results closely match previously published experimental data and that the arm model is

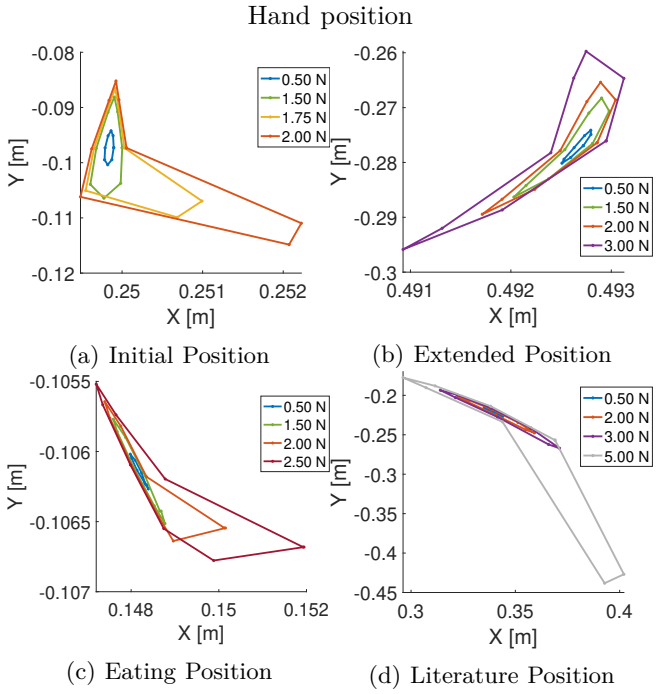

(a) Initial Position (b) Extended Position

(c) Eating Position (d) Literature Position

Fig. 4: Final hand position (x- and y-coordinates) for each arm configuration after an external force perturbation was applied for 100 ms. Higher forces lead to even higher and more distorted displacements, here not shown for clarity.

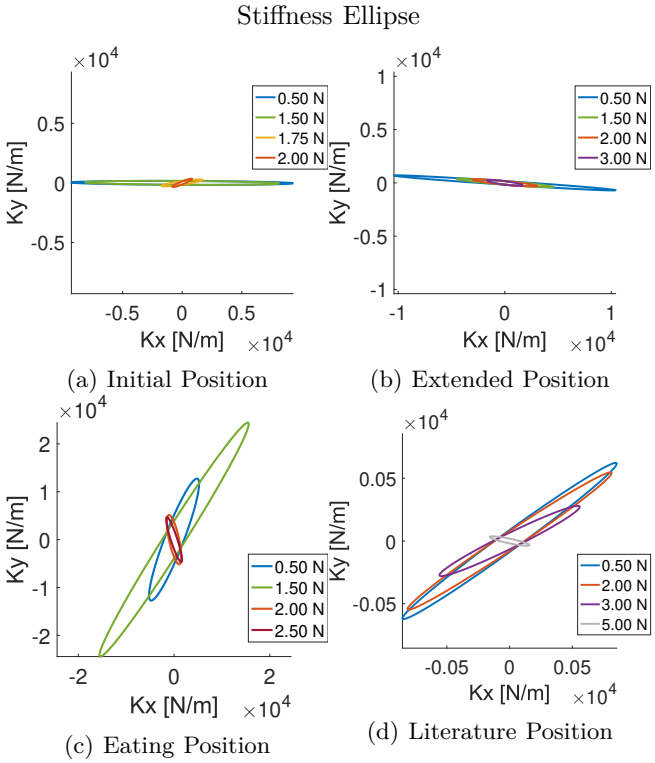

(a) Initial Position (b) Eating Position

(c) Eating Position (d) Literature Position

Fig. 5: Stiffness ellipses for each arm configuration. Higher forces lead to even higher and more distorted displacements, here not shown for clarity.

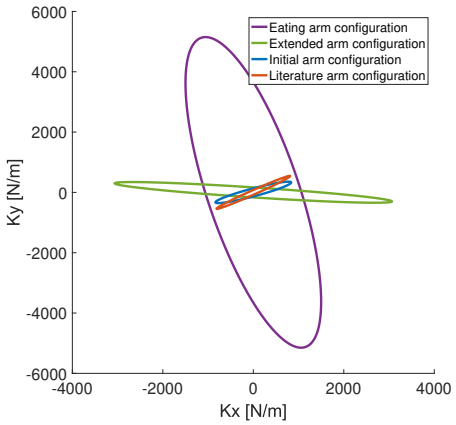

Fig. 6: Stiffness ellipses obtained from the different arm configurations for a reference perturbation level of 2 N.

able to replicate impedance values for existing literature values. Notably, previous experimental findings [3], [4], [21] have drawn similar conclusions about the trends of the stiffness ellipse orientation, findings that were corroborated in our study. Specifically, our evaluation of stiffness characteristics, with 2 N as the reference perturbation value, indicated that the range, orientation, and shape of stiffness ellipses closely mirror findings reported in the literature (see Fig 2).

Additionally, we showed that for different arm configurations, the same perturbation force leads to variations in stiffness ellipses regarding their size, orientation, and shape. In line with the experimental results of [11], [22], the major axes of the stiffness ellipses tend to be oriented toward the subject's shoulder, in our case, for example, along the x-axis for the extended position which is orientated towards the shoulder (see green curve in Fig. 6). Moreover, both experimental and numerical studies [8], [11], [22] have shown that stiffness ellipses tend to be more elongated towards the distal boundaries of the workspace and become more isotropic (more circular) toward proximal or more medial and posterior positions. In our results we also find a more isotropic ellipse in the eating configuration (Fig. 6, purple ellipse). Finally, in more medial and posterior stating positions, such as the eating configuration in our case, the size of the stiffness ellipses is larger, confirming higher hand restoring forces (see purple line in Fig. 6 and [8]).

Varying the perturbation force level showed that, up to a certain level, the larger the applied force, the larger the resulting hand displacement (see Fig. 3b, and Fig. 5) and the smaller the stiffness ellipses. Interestingly, the representation of impedance characteristics using stiffness ellipses was only reasonable for force perturbation levels up to 2 N, as shown by the coefficient of determination (R^2) indicating how well the characteristics could be explained using the stiffness ellipse representation. For larger force levels, we observed that the R^2 drops below 0.8, and in some cases, additional forces occur due to the joint

limit constraints (see Table III). This indicated that the stiffness ellipse representation was inadequate to predict corrective forces beyond this threshold. Consequently, our study emphasized the need for employing model-based approaches to estimate impedance in assistive devices. Models allow for predicting force responses for larger force ranges, thereby addressing the limitations posed by the existing stiffness ellipse representations.

Although we demonstrated that our numerical arm model predicts human impedance characteristics closely aligned with experimental studies, our approach had some limitations due to simplifications of the neuromusculoskeletal model compared to the human arm. While the MuJoCo arm model allows for computationally efficient real-time calculations, it employs a Hill-type muscle model that neglects tendon elasticity [10], [23] and short-range stiffness [24]. We expect that these simplifications influencing our results predominantly in large perturbations where tendon elasticity may become more relevant and in very fast and small perturbations, where the current muscle models underestimate the force [23], [25]. Furthermore, our use of an open-loop strategy to control the equilibrium positions of the arm neglected spinal reflexes. Although we determined muscle activation patterns heuristically and did not specifically consider the influence of co-contraction [21], the results still matched the literature (Fig. 2). Lastly, despite experimental evidence [3], [4] suggesting that the size of the ellipses fluctuates among human subjects due to variance in the muscle activation, joint configuration and the muscle length-tension relationship, our results did not account for individual characteristics, given that our numerical setup is currently purely deterministic.

In conclusion, we have shown that the investigated arm model in MuJoCo can predict stiffness values in alignment with experimental studies. In the future, we will use this computationally efficient model to predict corrective forces for assistive devices in real-time.

References

[1] T. Flash and F. Mussa-Ivaldi, "Human arm stiffness characteristics during the maintenance of posture," Experimental brain research, vol. 82, pp. 315–326, 1990.

[2] N. Hogan, "The mechanics of multi-joint posture and movement control," Biological cybernetics, vol. 52, no. 5, pp. 315–331, 1985.

[3] T. Flash and N. Hogan, "The coordination of arm movements: an experimentally confirmed mathematical model," Journal of neuroscience, vol. 5, no. 7, pp. 1688–1703, 1985.

[4] M. Darainy, N. Malfait, P. L. Gribble, F. Towhidkhah, and D. J. Ostry, "Learning to control arm stiffness under static conditions," Journal of neurophysiology, 2004.

[5] J. Friedman and T. Flash, "Task-dependent selection of grasp kinematics and stiffness in human object manipulation," Cortex, vol. 43, no. 3, pp. 444–460, 2007.

[6] S. Stroeve, "Impedance characteristics of a neuromusculoskeletal model of the human arm i. posture control," Biological cybernetics, vol. 81, no. 5-6, pp. 475–494, 1999.

[7] X. Hu, W. M. Murray, and E. J. Perreault, "Muscle short-range stiffness can be used to estimate the endpoint stiffness of the human arm," Journal of neurophysiology, vol. 105, no. 4, pp. 1633–1641, 2011.

[8] M. Asgari and D. L. Crouch, "Estimating human upper limb impedance parameters from a state-of-the-art computational neuromusculoskeletal model," in 2021 43rd Annual International Conference of the IEEE Engineering in Medicine & Biology Society (EMBC). IEEE, 2021, pp. 4820–4823.

[9] E. Todorov, T. Erez, and Y. Tassa, "Mujoco: A physics engine for model-based control," in 2012 IEEE/RSJ international conference on intelligent robots and systems. IEEE, 2012, pp. 5026–5033.

[10] A. Ikkala, F. Fischer, M. Klar, M. Bachinski, A. Fleig, A. Howes, P. Hämäläinen, J. Müller, R. Murray-Smith, and A. Oulasvirta, "Breathing life into biomechanical user models," in Proceedings of the 35th Annual ACM Symposium on User Interface Software and Technology, ser. UIST '22. New York, NY, USA: Association for Computing Machinery, 2022.

[11] T. Tsuji, P. G. Morasso, K. Goto, and K. Ito, "Human hand impedance characteristics during maintained posture," Biological cybernetics, vol. 72, pp. 475–485, 1995.

[12] A. Takagi, G. Xiong, H. Kambara, and Y. Koike, "Endpoint stiffness magnitude increases linearly with a stronger power grasp," Scientific reports, vol. 10, no. 1, p. 379, 2020.

[13] E. J. Perreault, R. F. Kirsch, and P. E. Crago, "Voluntary control of static endpoint stiffness during force regulation tasks," Journal of neurophysiology, vol. 87, no. 6, pp. 2808–2816, 2002.

[14] D. Piovesan, A. Pierobon, P. DiZio, and J. R. Lackner, "Experimental measure of arm stiffness during single reaching movements with a time-frequency analysis," Journal of neurophysiology, vol. 110, no. 10, pp. 2484–2496, 2013.

[15] J. M. Dolan, M. B. Friedman, and M. L. Nagurka, "Dynamic and loaded impedance components in the maintenance of human arm posture," IEEE transactions on systems, man, and cybernetics, vol. 23, no. 3, pp. 698–709, 1993.

[16] H. Gomi and M. Kawato, "Human arm stiffness and equilibrium-point trajectory during multi-joint movement," Biological cybernetics, vol. 76, no. 3, pp. 163–171, 1997.

[17] E. Burdet, R. Osu, D. Franklin, T. Yoshioka, T. Milner, and M. Kawato, "A method for measuring endpoint stiffness during multi-joint arm movements," Journal of biomechanics, vol. 33, no. 12, pp. 1705–1709, 2000.

[18] K. R. Saul, X. Hu, C. M. Goehler, M. E. Vidt, M. Daly, A. Velisar, and W. M. Murray, "Benchmarking of dynamic simulation predictions in two software platforms using an upper limb musculoskeletal model," Computer Methods in Biomechanics and Biomedical Engineering, vol. 18, no. 13, pp. 1445–1458, 2015, pMID: 24995410.

[19] C. F. Van Loan and G. Golub, "Matrix computations (johns hopkins studies in mathematical sciences)," Matrix Computations, vol. 5, 1996.

[20] A. Ikkala and P. Hämäläinen, "Converting biomechanical models from opensim to mujoco," in Converging Clinical and Engineering Research on Neurorehabilitation IV: Proceedings of the 5th International Conference on Neurorehabilitation (ICNR2020), October 13–16, 2020. Springer, 2022, pp. 277–281.

[21] H. Patel, G. O'Neill, and P. Artemiadis, "On the effect of muscular cocontraction on the 3-d human arm impedance," IEEE Transactions on Biomedical Engineering, vol. 61, no. 10, pp. 2602–2608, 2014.

[22] F. A. Mussa-Ivaldi, N. Hogan, and E. Bizzi, "Neural, mechanical, and geometric factors subserving arm posture in humans," Journal of neuroscience, vol. 5, no. 10, pp. 2732–2743, 1985.

[23] M. Millard, T. Uchida, A. Seth, and S. L. Delp, "Flexing computational muscle: modeling and simulation of musculotendon dynamics," Journal of biomechanical engineering, vol. 135, no. 2, p. 021005, 2013.

[24] T. Siebert, H. R. Screen, and C. Rode, "Computational modelling of muscle, tendon, and ligaments biomechanics," in Computational modelling of biomechanics and biotribology in the musculoskeletal system. Elsevier, 2021, pp. 155–186.

[25] L. Cui, E. J. Perreault, H. Maas, and T. G. Sandercock, "Modeling short-range stiffness of feline lower hindlimb muscles," Journal of Biomechanics, vol. 41, no. 9, pp. 1945–1952, 2008.